THE JOURNAL OF PHYSICAL CHEMISTRY C

Article

pubs.acs.org/JPCC

Nano-nitride Cathode Catalysts of Ti, Ta, and Nb for Polymer Electrolyte Fuel Cells: Temperature-Programmed Desorption Investigation of Molecularly Adsorbed Oxygen at Low Temperature

Ryohji Ohnishi,[†] Kazuhiro Takanabe,[‡] Masao Katayama,[†] Jun Kubota,[†,§] and Kazunari Domen*[,†]

[†]Department of Chemical System Engineering, The University of Tokyo, 7-3-1 Hongo, Bunkyo-ku, Tokyo 113-8656, Japan

[‡]Division of Physical Sciences and Engineering, KAUST Catalysis Center (KCC), King Abdullah University of Science and Technology (KAUST), 4700 KAUST, Thuwal 23955-6900, Saudi Arabia

[§]Elements Strategy Initiative for Catalysts and Batteries (ESICB), Kyoto University Katsura, Kyoto 615-8520, Japan

ABSTRACT: TiN, NbN, TaN, and Ta_3N_5 nanoparticles synthesized using mesoporous graphitic (mpg)-C_3N_4 templates were investigated for the oxygen reduction reaction (ORR) as cathode catalysts for polymer electrolyte fuel cells. The temperature-programmed desorption (TPD) of molecularly adsorbed O_2 at 120−170 K from these nanoparticles was examined, and the resulting amount and temperature of desorption were key factors determining the ORR activity. The size-dependent TiN nanoparticles (5−8 and 100 nm) were then examined. With decreasing particle size, the density of molecularly adsorbed O_2 per unit of surface area increased, indicating that a decrease in particle size increases the number of active sites. It is hard to determine the electrochemical active surface area for nonmetal electrocatalysts (such as oxides or nitrides), because of the absence of proton adsorption/desorption peaks in the voltammograms. In this study, O_2-TPD for molecularly adsorbed O_2 at low temperature demonstrated that the amount and strength of adsorbed O_2 were key factors determining the ORR activity. The properties of molecularly adsorbed O_2 on cathode catalysts are discussed against the ORR activity.

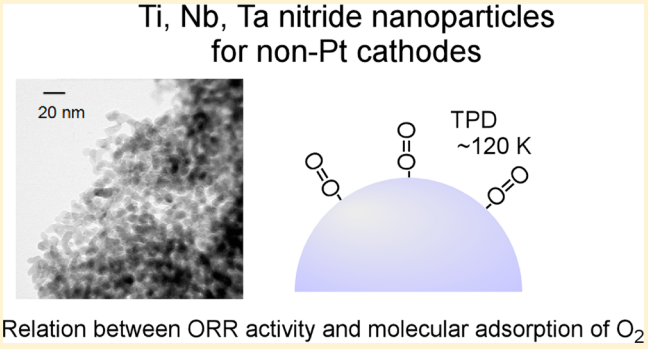

Relation between ORR activity and molecular adsorption of O_2

1. INTRODUCTION

Polymer electrolyte fuel cells (PEFCs) have attracted considerable attention as clean generators of electricity due to their high energy-conversion efficiency, relatively low operating temperature, and high power density.[1,2] PEFCs are thus promising for use in fuel cell vehicles (FCVs) and residential cogeneration systems. All commercial PEFCs to date have employed a large amount of Pt or Pt alloy as an electrocatalyst, especially as a cathode to catalyze the oxygen reduction reaction (ORR), and the performance of the cathode is still the primary limitation of overall PEFC efficiency. Platinum is a precious metal with limited reserves available on the Earth, so the widespread commercialization of Pt-based PEFCs would be unrealistic. The stability of Pt and Pt alloy catalysts also becomes a serious problem in long-term operation, because these catalysts can dissolve into the polymer electrolyte in acidic and oxidizing environments, after which the dissolved Pt will precipitate in the ionomer layer and damage the ionomer.[3,4] The widespread application of PEFCs therefore requires electrocatalysts based on naturally abundant elements that are stable in acidic media. A strong motivation exists to develop noble-metal alternatives that are more tolerant to acidic conditions than Pt and related materials and that exhibit a comparable catalytic activity for the ORR.

Various materials have been investigated for non-noble-metal cathode catalysts. The first example was a catalyst consisting of transition-metal Fe or Co complexes dispersed in macrocyclic structures such as porphyrin, phenanthroline, phthalocyanine, polyacrylonitrile, polypyrrole, or polyaniline.[5−15] Later, carbon-based materials, even without transition metals, especially when doped with nitrogen, were reported to exhibit excellent ORR activity.[16−21] Nevertheless, none of these electrocatalysts has reached the catalytic activity of Pt-based electrocatalysts, and stability in an acidic environment remains an unsolved issue. Another approach for developing non-noble-metal cathodes is the use of groups IV and V transition metals, because of their abundance and high stability in acidic media.[22−34] Ota et al. reported that partially oxidized TaC_xN_y, ZrC_xN_y, and NbC_xN_y showed onset potentials for the ORR comparable to those of Pt-based catalysts while remaining highly stable under PEFC cathode conditions.[24−26] Until recently, because the synthesis of these catalysts required high-temperature treatment, only bulky, low surface area particles were produced with diameters up to 100 nm, resulting in low current densities.

Received: November 6, 2012
Revised: December 12, 2012
Published: December 12, 2012

To achieve higher ORR performance, the active sites of the catalyst should be well dispersed on an electrically conductive support material with a large surface area. We have therefore investigated several synthetic methods to produce nano- or subnanosized ORR catalysts well dispersed on carbon black (CB) powders.[23−29] First, an arc plasma method was used to produce subnanosized Nb−oxynitride-like materials by controlling the gas atmosphere (N_2 and O_2).[28] Second, a polymer complex (PC) method in solution phase was utilized to prepare well-dispersed catalysts of Ba−Nb, Ba−Zr, and Fe−Ti on CB.[29−31] Recently, electrodeposition from a nonaqueous electrolyte bath has been established for preparation of Ta cathode catalysts with nanoscale dispersion.[32] Alternatively, titanium nitride (TiN) nanoparticles prepared using mesoporous graphitic (mpg)-C_3N_4 templates have been investigated as nanosized ORR catalysts.[33] Direct synthesis of TiN nanoparticles on CB or few-walled carbon nanotubes (FWCNT) was established using the respective carbon/mpg-C_3N_4 composites for improved ORR performance.[34] The presence of CB or FWCNTs, which have high electrical conductivity, drastically enhanced the ORR current. Throughout this research, we have considered the TiN surfaces to be at least partially oxidized once they are exposed to air and the active sites to be oxygen vacancies or defect sites, which should facilitate the adsorption of molecular oxygen. One problem for the oxide/nitride catalysts of groups IV and V transition metals is hydrogen peroxide formation is more obvious than Pt catalysts. Several percentage of hydrogen peroxide was detected by rotating ring-disk electrode (RRDE) measurement.[29,35] However, most of reaction path is four electron reduction, and it can be solved by the electrode design.

The active sites of oxide and nitride cathode catalysts for the ORR have not been investigated sufficiently, but Pt electrodes have been well investigated,[36] even for surface science approaches using single-crystal surfaces. For Pt-based catalysts, the active-site density can be determined using an electrochemical surface area (ECSA) estimated from the proton adsorption/desorption peak areas in voltammograms.[36] The oxygen adsorption/desorption peaks in voltammograms are also characteristic for Pt-based catalysts. However, in the case of oxide or nitride cathode catalysts, there are no specific adsorption/desorption peaks in the voltammograms. Although the absence of specific adsorption/desorption indicates that these materials are quite stable in the electrolyte, the absence of information on the ECSA of these materials makes it difficult to understand the intrinsic activity of the active surfaces. Electric double-layer capacitance (EDLC) is one indicator, but this only indicates the total surface area of electrically conductive catalyst. The density of the active sites is independent of the EDLC. The values calculated from the EDLC are similar to those obtained from Brunauer−Emmett−Teller (BET) specific surface area measurements based on N_2 adsorption.

The first elemental step of the ORR is the adsorption of molecular oxygen on the catalyst surface.[37−41] The molecularly adsorbed oxygen is next protonated forming an O−H bond with an electron. After that, the O−O bond is dissociated for further reduction to H_2O. If the O−O bond is not dissociated, undesirable H_2O_2 is obtained. In both cases, molecularly adsorbed oxygen is the precursor of the ORR. The investigation of molecularly adsorbed oxygen on cathode catalysts should provide essential information regarding ORR performance. Temperature-programmed desorption (TPD) measurements have been widely utilized to estimate the amount of adsorbates and the strength of adsorption on surfaces.[42−48] TPD spectra of oxygen on Pt surfaces have been well investigated.[39,40] Gland et al. reported that the desorption peak of molecular oxygen from a Pt(111) surface appeared at 100−150 K, and that of atomic (dissociated) oxygen appeared above 400−600 K.[44,45] To utilize the O_2-TPD experiments, we can expect to obtain useful information regarding the adsorption sites of oxygen on the cathode catalysts, even for oxide or nitride catalysts.

In this study, we investigated the ORR properties of TiN, NbN, TaN, and Ta_3N_5 nanoparticles as cathode catalysts for PEFCs. The O_2-TPD behavior at low temperatures was compared with the trend in ORR performance. It indicates that the molecular adsorption of O_2 on ORR catalysts provides useful knowledge for improving ORR performance.

2. EXPERIMENTAL SECTION

2.1. Catalyst Synthesis. TiN nanoparticles were prepared using mpg-C_3N_4 templates, as reported previously.[32,49] Briefly, TiN nanoparticles with different particle sizes were prepared using mpg-C_3N_4 with different pore sizes. In this study, three kinds of aqueous silica solutions (LUDOX SM-30, HS-40, TM-40; Aldrich) that contained 7, 12, and 23 nm silica spheres, respectively, were used to vary the pore size of the mpg-C_3N_4 templates. A cyanamide (CA; 99%, Aldrich) precursor was dissolved in the solution to achieve a weight ratio of unity between cyanamide and silica, and then, the mixture was heated to 343 K with stirring to ensure slow evaporation of the water. The resulting solid was heated in a closed ceramic crucible at a rate of 2.3 K min^{-1} for 4 h to reach 823 K, and it was held at this temperature for 4 h. Removal of the silica by washing with a 4 M NH_4HF_2 solution yielded a mpg-C_3N_4 template. Titanium(IV) chloride (1.08 g; Wako Chemicals) was slowly dissolved in 2.0 g of ethanol. To this solution, 1.35 g of the prepared mpg-C_3N_4 was added. After 1 h, complete penetration of the solution into the mesoporous framework was assumed. The infiltrated mpg-C_3N_4 was collected by suction filtration and washed with ethanol. The resulting powder was heated in a tubular furnace at a rate of 3.25 K min^{-1} over 4 h to 1073 K, and then, it was kept at this temperature for 3 h under N_2 flow. When the temperature was lowered to room temperature, 1% O_2/He gas was slowly introduced into the furnace before the samples were exposed to air. For Ta and Nb nitride nanoparticles, 12 nm silica spheres were used for the synthesis of mpg-C_3N_4, and as metal precursors, $TaCl_5$ (2.04 g; Wako Chemicals) or $NbCl_4$ (1.54 g; Wako Chemicals) were used, respectively. For Ta, N_2 and NH_3 flows were used to synthesize TaN and Ta_3N_5, respectively. In the case of N_2 flow, the samples were heated in the same condition as TiN, whereas under NH_3 flow, the powder was heated to 973 K and then kept at this temperature for 3 h. The detailed procedure for Ta and Nb nitride nanoparticles was described in refs 50 and 51.

As an Fe-containing reference electrode catalyst, an Fe-based Ti-containing catalyst was prepared by the PC method, as described in our previous paper.[31] The catalysts were prepared using 1,10-phenanthroline and NH_3 gas as the nitrogen source and formed Fe-based active sites for ORR. As Pt-based catalysts, Pt/CB (39.4 wt %; Ishifuku, FC-I1) was used, while 2 wt % Pt/Al_2O_3 (BEL JAPAN; Pt surface area: 73.6 m^2 g^{-1}, 0.08 nm^2 $atom^{-1}$) was used for O_2-TPD measurements. Carbon black (CB; Vulcan, XC-72R), Al_2O_3, and SiO_2 were also used for reference.

2.2. Electrochemical Measurements. Inks of the powder catalysts were prepared as follows. A portion of the prepared

dx.doi.org/10.1021/jp3109573 | J. Phys. Chem. C 2013, 117, 496−502

catalyst (5 mg) was suspended in a mixture of 973 μL of isopropanol, 472 μL of distilled water, and 1.14 μL of 5% Nafion solution (Sigma−Aldrich) under ultrasonication for 15 min. For the measurements in acidic media, carbon paper (Toray TGP-H-120) or a rotating disk electrode (RDE) was used as the working electrode. An aliquot of 289 μL of the suspension was dropped onto a carbon paper in an area of 1 cm^2, and 36.3 μL of the suspension was dropped onto a ϕ4 grassy carbon disk of RDE.

Electrochemical measurements were conducted in 100 mL of 0.1 M H_2SO_4 aqueous solution at 298 K using a potentiostat (HSV-100 or HZ-5000; Hokuto Denko). For RDE measurement, RRDE-3 (BAS) was used. A carbon rod and a Ag/AgCl electrode were used as the counter and reference electrodes, respectively. The Ag/AgCl electrode was calibrated using a reversible hydrogen electrode (RHE), which consisted of a Pt electrode and hydrogen gas at 1 atm, and the potentials in this paper are expressed against the RHE. After bubbling with Ar for 30 min to remove dissolved O_2, reduction oxidation cycles were conducted between 0.11 and 1.23 V_{RHE} at a scan rate of ±5 mV s^{-1} at 298 K. The oxidation and reduction cycles were usually repeated 10 times to ensure stabilization of the sample electrode. To examine ORR performance, linear-sweep voltammograms were recorded from 1.23 V_{RHE} at a scan rate of −5 mV s^{-1} after bubbling with Ar or O_2 gas for 30 min.

2.3. O_2-TPD Measurements. Adsorption of O_2 on ORR catalysts was investigated using O_2-TPD measurements. A schematic view of the apparatus is shown in Figure 1. The

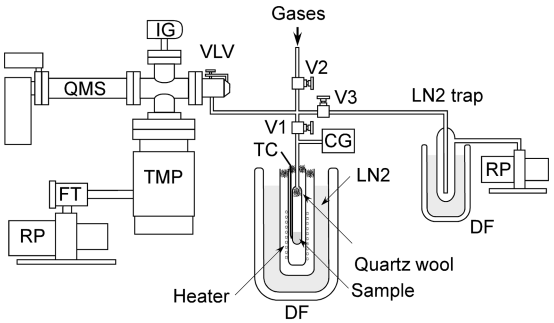

RP : Mechanical rotary pump
FT : Fore line trap
TMP : Turbo molecular pump
QMS : Quadro-pole mass spectrometer
IG : Bayard-Alpert ionization gauge
VLV : Variable leak valve
V1-V3 : Metal bellows valves
CG : Capacitance pressure gauge
TC : Thermocouple
LN2 : Liquid nitrogen
DF : Dewar flask

Figure 1. Apparatus for TPD measurements of molecularly adsorbed oxygen at liquid nitrogen temperature.

sample, in an amount corresponding to a surface area of 1.25 m^2, was set in a glass tube, and the temperature of the tube was measured by a thermocouple bound to the tube. The temperature was controlled using a furnace around the tube, and the furnace was cooled by liquid nitrogen in a Dewar vessel. All samples in their glass tubes were first treated at 473 K in vacuum using a rotary pump to remove adsorbed water, then treated in 10 kPa of H_2 at 673 K for 1 h, followed by treatment in vacuum at 673 K for 1 h to remove the impurities at the surface. Pretreated samples were cooled to 93 K in vacuum, and then, 1 kPa of O_2 (99.9999%) was introduced to adsorb on the samples. After a while, the sample tube was evacuated to 5 × 10^{-5} Pa by a turbomolecular pump. The temperature of the sample was raised monotonically at a heating rate of 5 K min^{-1} in the range 93−473 K. The desorbing gas was monitored by a quadrupole mass spectrometer (QMS; ANELVA AQA-100). The signal for m/e equals 1−50 was recorded.

2.4. Catalyst Characterization. The crystal structures of the samples were investigated by X-ray diffraction (XRD; RINT-UltimaIII, Rigaku), and transmission electron microscopy (TEM; TITAN ST, FEI) was used to observe the morphology. The BET surface area was measured using a BELSORP-mini system (BEL JAPAN).

3. RESULTS AND DISCUSSION

3.1. Comparison of Pt/CB, Ti−Fe−O−N/CB, TiN, and CB. ORR voltammograms of Pt/CB, Ti−Fe−O−N/CB, TiN, and CB in 0.1 M H_2SO_4 are shown in Figure 2. In this figure,

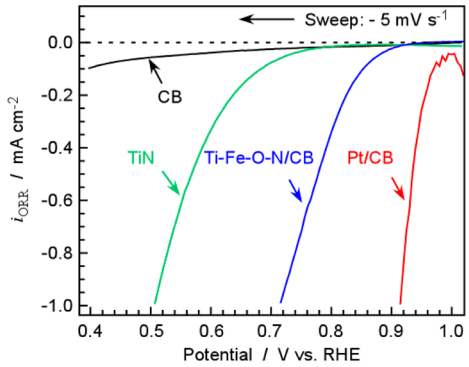

Figure 2. Voltammograms of ORR for Pt/CB, Ti−Fe−O−N/CB, and TiN catalysts in 0.1 M H_2SO_4.

TiN catalyst synthesized from a 12 nm template was used. The vertical axis shows the difference in currents measured in O_2 and Ar atmospheres. While the Pt catalyst generated an ORR current at an onset potential of 1.0 V_{RHE}, the Fe−Ti and TiN catalysts had onset potentials of 0.9 and 0.75 V_{RHE}, respectively. The Ti−Fe catalyst generated a higher ORR current than the TiN catalyst; however, the durability of the Ti−Fe catalyst has been reported to be problematic. Note that the TiN nanoparticles in the present work did not have the high activity reported in our previous work.[33] In the present work, bare TiN nanoparticles were used without compositing with CB, because the ORR and O_2 adsorption properties of TiN should be solely examined. Composites of TiN and CB have been reported to have higher activity.

TPD spectra of oxygen from Pt/Al_2O_3, Ti−Fe−O−N/CB, TiN, and CB catalysts are shown in Figure 3. Al_2O_3 was also measured for reference. Only O_2 desorption was observed in the m/e range between 1 and 50, except for the negligible amount of H_2O desorption around 200−300 K. It should be noted that the intensity in the vertical axis was normalized by the BET surface area of the catalysts. For commercial Pt/Al_2O_3, the signal was normalized by the area of the Pt surface, which is reported by the supplier company to be 73.6 m^2 g^{-1}. Because the vertical axis was normalized by the BET surface areas of these materials, the area intensity of a desorption peak indicates the amount of adsorbed O_2 per unit BET area.

For Pt/Al_2O_3, an O_2 desorption peak was observed at 170 K. The absence of an O_2 desorption peak for Al_2O_3 indicated that

dx.doi.org/10.1021/jp3109573 | J. Phys. Chem. C 2013, 117, 496−502

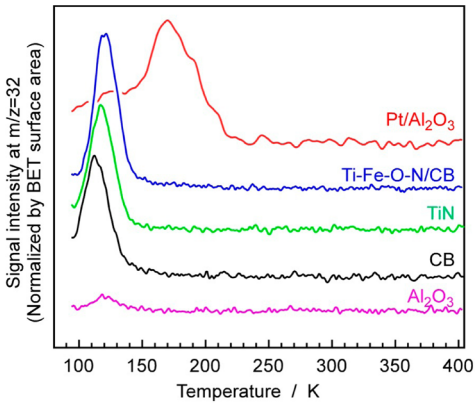

Figure 3. TPD spectra of oxygen from Pt/CB, Ti−Fe−O−N/CB, and TiN catalysts. Oxygen was adsorbed at 95 K, and the heating rate was 5 K min^{-1}.

O_2 molecules were adsorbed on the Pt surface. The amounts of O_2 adsorption estimated from the TPD are listed in Table 1,

Table 1. BET Surface Area and Adsorption Density of Molecular Oxygen Estimated from O_2-TPD for Various Cathode Catalysts

sample	BET area (m^2 g^{-1})	O_2 adsorption density (molecules nm^{-2})
Pt/Al_2O_3	73.6[a]	2.1
TiN (7 nm[b])	330	0.57
TiN (12 nm[b])	256	0.52
TiN (23 nm[b])	154	0.18
TiN (100 nm)	5	not detected
Ti−Fe−O−N/CB	348	0.60
CB (Vulcan XC-72R)	240	0.54

[a]Area of Pt surface. [b]The sizes indicated are the size of SiO_2 templates, and the actual sizes of TiN nanoparticles are explained in the main text.

which summarizes all of the samples in the present work. This desorption of O_2 below 200 K can be assigned to molecularly adsorbed O_2 on the basis of surface scientific knowledge. In the case of Pt(111), the amount of adsorbed molecular O_2 has been reported to be 4.1 molecules nm^{-2}.[44] In this study, the amount of O_2 adsorption on Pt/Al_2O_3 was estimated to be 2.1 molecules nm^{-2}, which was obviously lower than the value for Pt(111). Two possible reasons for this difference were considered. First, the practical catalysts in this work were not as clean as an ideal Pt(111) single-crystal surface. Furthermore, the Pt particles in the practical catalyst did not consist of only Pt(111), so the difference in adsorption is reasonable. The other reason for the difference is that the temperature of our apparatus was not sufficiently low to achieve saturation. The first reason was probably dominant in the case of Pt/Al_2O_3, because the adsorption temperature of 95 K was much lower than the desorption temperature of 170 K. For non-Pt cathode catalysts in this work, the measured amount of adsorption was smaller than the saturation amount primarily because the adsorption temperature is close to the desorption temperature. Nevertheless, it is still useful to compare the relative amounts of adsorption among the catalyst samples.

For Ti−Fe−O−N/CB, TiN, and CB catalysts, O_2 desorption peaks were observed around 120 K. The desorption peaks shifted to lower temperatures in the order of Ti−Fe−O−N/CB, TiN, and CB, indicating weakening O_2 adsorption in this order. The amounts of adsorption per unit surface area for these cathode catalysts are also in the same order. This suggests that the cathode catalysts with higher amounts of O_2 adsorption and/or with higher desorption temperatures have higher ORR activities. There is no doubt that Pt is the best cathode catalyst among those we examined, and both the amount of O_2 adsorption and the temperature of O_2 desorption for Pt were the highest among these samples.

The TPD spectra can be simulated by the Polanyi−Wigner equation as follows:

$$r_d = -\frac{d\theta}{dt} = k_d\theta^n = k_0\theta^n \exp\left[\frac{-E_A}{RT}\right]$$

where r_d, θ, t, k_d, n, k_0, E_A, R, and T are the rate of desorption, time, the rate constant of desorption, the reaction order, a pre-exponential factor, the activation energy for desorption, the gas constant, and temperature.[41,42] The activation energy for desorption almost equals the heat of adsorption, especially for nondissociative adsorption. For molecular adsorption of oxygen, n can reasonably be considered to be unity. Assuming a k_0 value of 1×10^{12} s^{-1}, we estimated E_A values as 45 kJ mol^{-1} for Pt/Al_2O_3, 32 kJ mol^{-1} for Ti−Fe−O−N/CB, 30 kJ mol^{-1} for TiN, and 26 kJ mol^{-1} for CB. The E_A value of molecular oxygen on Pt(111) has been reported to be 37 ± 2 kJ mol^{-1} (at least in the high-coverage limit).[43] Considering that the surface of a Pt particle consists of less-packed crystal faces with various steps, the obtained value of 45 kJ mol^{-1} for Pt/Al_2O_3 is reasonable. The heats of adsorption of molecular oxygen for Ti−Fe−O−N/CB, TiN, and CB were lower than that for Pt/Al_2O_3. The heat of condensation of oxygen was 6.8 kJ mol^{-1}, and the heats of adsorption of molecular oxygen for Ti−Fe−O−N/CB, TiN, and CB were obviously higher than the heat of condensation, indicating that this adsorption should be classified as chemisorption. The order of heat of adsorption of molecular oxygen corresponded to that of ORR performance. It can reasonably be imagined that stronger oxygen adsorption results in higher oxygen coverage at the catalyst surface, leading to higher ORR performance. At this point, the development of non-Pt catalysts with stronger adsorption of molecular oxygen is one promising means of improving ORR performance.

3.2. Ti, Ta, and Nb Nitride Nanoparticles. Ti-, Ta-, and Nb-based nanoparticles were synthesized, and the XRD patterns are shown in Figure 4. The Ta(III) nitride TaN was obtained by nitridation with mpg-C_3N_4 under N_2 flow, while the Ta(V) nitride Ta_3N_5 was obtained under NH_3 flow. From the XRD peak width, the crystal sizes of these nanoparticles were determined to be <5 nm (TiN), 6 nm (NbN), and 14 nm (Ta_3N_5). It was difficult to apply Scherrer's equation to the XRD pattern of TaN because of its broadness. Figure 5 shows TEM images of NbN, TaN, and Ta_3N_5 particles. These particles appeared to consist of particles several nanometers in size. For TiN, the TEM images were shown in our previous papers.

It was found that all of these nitride nanoparticles had ORR activity, as shown in Figure 6. Among TiN, NbN, TaN, and Ta_3N_5, TiN showed the highest onset potential for the ORR of around 0.75 V_{RHE}. Ta_3N_5 also showed an onset potential for the ORR around 0.75 V_{RHE}; however, the current was somewhat limited. The TaN nanoparticles produced the lowest current in the ORR.

dx.doi.org/10.1021/jp3109573 | J. Phys. Chem. C 2013, 117, 496−502

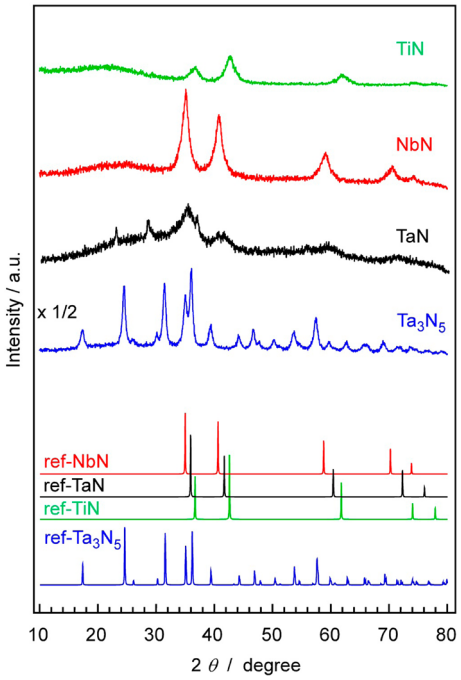

Figure 4. XRD patterns of TiN, NbN, TaN, and Ta_3N_5 nanoparticles.

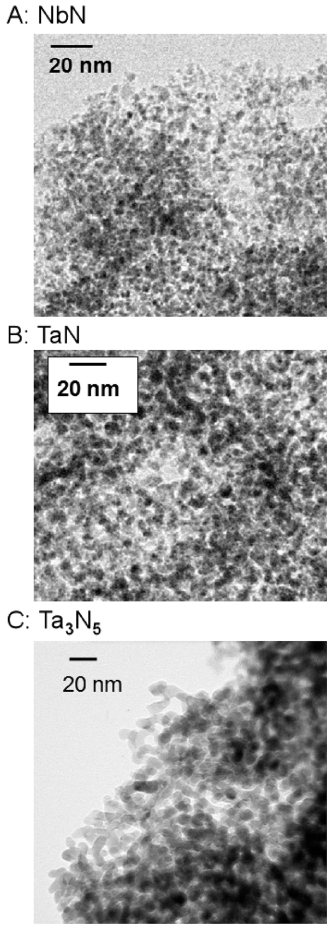

Figure 5. TEM images of TiN, NbN, TaN, and Ta_3N_5 nanoparticles.

TPD spectra of O_2 from TiN, NbN, TaN, and Ta_3N_5 are shown in Figure 7. Corresponding to the trend in ORR activity, the desorption peak of O_2 from the TiN surface was the most

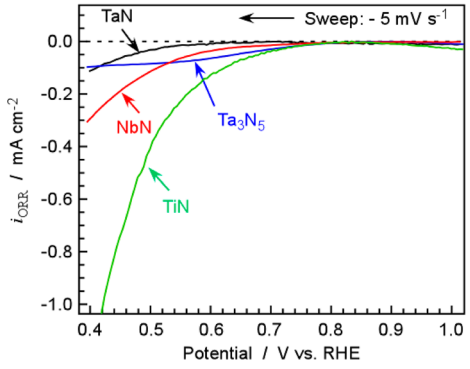

Figure 6. Voltammograms of the ORR for 20 wt % M/CB (M = TiN, NbN, TaN, or Ta_3N_5) nanoparticles in 0.1 M H_2SO_4. The revolution rate of RDE was 1600 rpm, and the sweep rate was −5 mV s^{-1} in the cathodic direction.

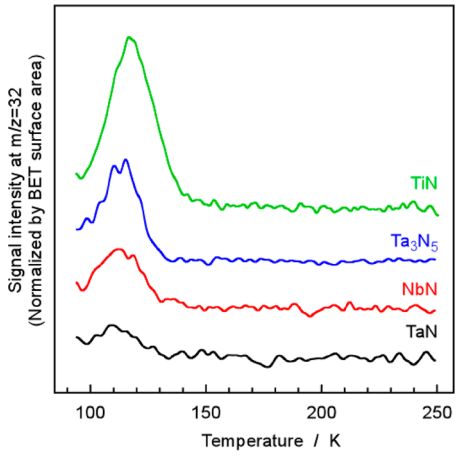

Figure 7. O_2-TPD spectra from TaN, TiN, NbN, and Ta_3N_5 nanoparticles. Oxygen was adsorbed at 95 K, and the heating rate was 5 K min^{-1}.

intense, indicating that TiN can adsorb the highest amount of O_2 among these samples.

3.3. Size Dependence of TiN Nanoparticles. Three sizes of TiN nanoparticles were synthesized by changing templates, as mentioned in the Experimental Section. The SiO_2 colloid templates used were 7, 12, and 23 nm in diameter. By applying Scherrer's equation to the XRD patterns, the sizes of the TiN nanoparticles were estimated to be <5 nm (7 nm template), <5 nm (12 nm template), and 8 nm (23 nm template). The detailed method of controlling the TiN particle size using mpg-C_3N_4 templates was published elsewhere.[33,34,49,52] The above particle sizes were confirmed by TEM. A commercial TiN (WAKO) powder, which has a particle size of approximately 100 nm as measured by scanning electron microscopy (SEM) was used as a reference.

Voltammograms for the ORR with TiN nanoparticles in 0.1 M H_2SO_4 using RDE are shown in Figure 8. Generally, smaller particles generated a higher ORR current. The onset potential did not depend on the particle size, indicating that the essential activity of TiN is common and that the number of active sites increases with decreasing particle size. It should be noted that the 7 nm TiN nanoparticles in acidic solution did not show clear ORR activity and the onset potential and ORR current were not consistent with the results from the other samples. This is because the 7 nm particles were not durable under

dx.doi.org/10.1021/jp3109573 | J. Phys. Chem. C 2013, 117, 496−502

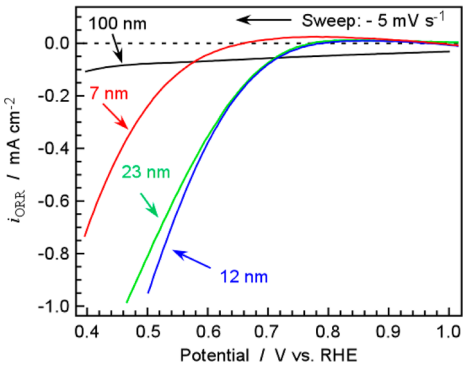

Figure 8. Voltammograms for the ORR of TiN catalysts with changing the size of nanoparticles in 0.1 M H_2SO_4. The revolution rate of RDE was 1600 rpm, and the sweep rate was −5 mV s^{-1} in the cathodic direction. The sizes indicated are the sizes of the SiO_2 templates. The actual sizes of the TiN nanoparticles are explained in the main text.

acidic conditions. As discussed in our previous paper, the surface of TiN nanoparticle catalysts is oxidized to form TiO_2 by acidic and high-potential condition. In the case of 7 nm particles, most of the particles are oxidized, and the activity of particles decreases drastically. For commercial TiN (100 nm) powder, no ORR current was observed.

TPD spectra of molecularly adsorbed oxygen were examined, as shown in Figure 9. The density of molecularly adsorbed O_2

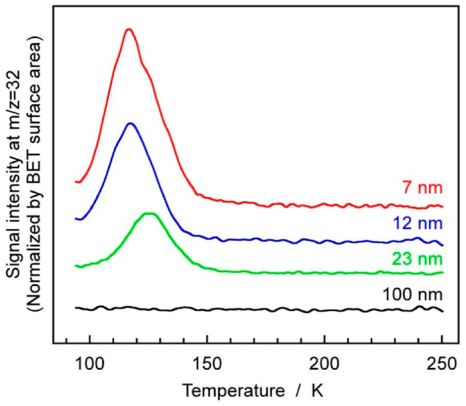

Figure 9. TPD spectra of oxygen from various sizes of TiN nanoparticles. The sizes indicated are the sizes of the SiO_2 templates. The actual sizes of the TiN nanoparticles are explained in the main text. Oxygen was adsorbed at 95 K, and the heating rate was 5 K min^{-1}.

per unit BET area was estimated and is listed in Table 1. The desorption peaks for all samples were positioned at 115−120 K, indicating the heat of adsorption of oxygen on these samples was constant. For commercial TiN with a low surface area, no desorption peak was observed. The amount of adsorption of oxygen per unit BET surface area increased with decreasing particle size. This indicates that the density of adsorption sites increases with decreasing particle size. It suggests that the decrease in particle size increases not only the surface area but also the site density. The number of step sites per unit surface area should increase with decreasing particle size, especially for nanocrystals. It should be also noted that the density of oxygen adsorption on TiN catalysts was less than one-quarter of that on Pt/CB. Fewer adsorption sites and weaker adsorption of O_2 would prevent non-Pt catalysts from achieving a high ORR activity.

3.4. General Discussion. The molecular adsorption of O_2 on Pt cathode catalysts has been known to be the first step in the elemental steps of the ORR.[37−41] The adsorbed O_2 can then react with protons and electrons to form OOH species. For oxide and nitride catalysts, dissociative adsorption of O_2 can be difficult, because the metal cation sites are isolated by O or N anions and the metal cations are already oxidized. This is possibly the reason why the hydrogen peroxide formation is more obvious than that for Pt catalysts.[29,35] Thus, the theory that adsorbed O_2 begins to be reduced by protons and electrons before dissociation seems more likely for oxide and nitride catalysts. Considering this reaction mechanism, the molecular adsorption of O_2 is necessary in the ORR, and the amount of adsorption of O_2 should reflect the current density of the ORR. In the case of oxide and nitride catalysts, the electric conductivity of the catalysts is sometimes limited. Even if the adsorption sites catch molecular O_2, the catalysts cannot reduce this O_2 when the adsorption sites are not conductive. It should be noted that the O_2-TPD measurements show the total amount of O_2 desorbed from both conductive and non-conductive sites. In other words, ORR catalysts require both adsorption of molecular O_2 and conductivity for electron migration. In this article, we demonstrate that there is a correlation between molecular adsorption of O_2 and ORR activity for various cathode catalysts. However, further study is required to reveal how much adsorbed O_2 can be reduced with receiving electrons.

The density of adsorption sites for molecular O_2 was in an important factor determining ORR activity. The molecular adsorption of O_2 investigated in this work was observed at relatively low temperatures of 120−170 K. The practical operating temperature of PEFCs is generally 343−353 K, and the amount of O_2 adsorption at these temperatures is negligible. Under such conditions, to increase the amount of adsorbed O_2, the heat of adsorption of O_2 is as important as the number of adsorption sites. The TPD peaks of O_2 from non-Pt catalysts in this work were obviously positioned at lower temperatures than that of Pt. Increasing the heat of adsorption, which would shift the peak of O_2-TPD higher, is a good strategy for catalyst development.

4. CONCLUSION

The properties of TiN, NbN, TaN, and Ta_3N_5 nanoparticles as cathode catalysts for PEFCs were investigated. TiN, NbN, TaN, and Ta_3N_5 nanoparticles were found to have ORR activity; especially, TiN and Ta_3N_5 showed an obvious ORR onset potential at 0.75 V_{RHE}. TPD spectra of molecularly adsorbed O_2 were measured for these cathode catalysts. From these nitride nanoparticles, a desorption peak was observed at 120 K, while a Pt cathode catalyst showed a peak at 170 K. For various sizes of TiN nanoparticles (5−100 nm), the density of molecularly adsorbed O_2 increased with decreasing particle size, indicating that the active sites appear on the surface of nanoparticles. The amount and strength of molecular adsorption of O_2 were concluded to strongly affect ORR activity. Higher adsorption amounts and stronger adsorption are very important for achieving a high ORR activity.

AUTHOR INFORMATION

Corresponding Author

*E-mail: domen@chemsys.t.u-tokyo.ac.jp.

dx.doi.org/10.1021/jp3109573 | J. Phys. Chem. C 2013, 117, 496−502

Notes

The authors declare no competing financial interest.

■ ACKNOWLEDGMENTS

This work is partly supported by Funding Program for World-Leading Innovative R&D on Science and Technology (FIRST) of Cabinet Office of Japan, the international exchange program of the A3 Foresight Program of the Japan Society for the Promotion of Science (JSPS), and "Elements Strategy Initiative to Form Core Rersearch Center" (since 2012), Ministry of Education Culture, Sports, Science and Technology (MEXT), Japan.

■ REFERENCES

(1) Carrette, L.; Friedrich, K. A.; Stimming, U. *Fuel Cells* **2001**, *1*, 5−39.
(2) Gasteiger, H. A.; Kocha, S. S.; Sompalli, B.; Wagner, F. T. *Appl. Catal., B* **2005**, *56*, 9−35.
(3) Borup, R.; Meyers, J.; Pivovar, B.; Kim, Y. S.; Mukundan, R.; Garland, N.; Myers, D.; Wilson, M.; Garzon, F.; Wood, D.; et al. *Chem. Rev.* **2007**, *107*, 3904−3951.
(4) Yu, P.; Pemberton, M.; Plasse, P. *J. Power Source* **2005**, *144*, 11−20.
(5) Jasinski, R. *Nature* **1964**, *201*, 1212−1213.
(6) Gupta, S. L.; Tryk, D.; Bae, I.; Aldred, W.; Yeager, E. B. *J. Appl. Electrochem.* **1989**, *19*, 19−27.
(7) Bashyam, R.; Zelenay, P. *Nature* **2006**, *443*, 63−66.
(8) Bezerra, C. W. B.; Zhang, L.; Lee, K.; Liu, H.; Marques, A. L. B.; Marques, E. P.; Wang, H.; Zhang, J. *Electrochim. Acta* **2008**, *53*, 4937−4951.
(9) Nallathambi, V.; Lee, J. W.; Kumaraguru, S. P.; Wu, G.; Popov, B. N. *J. Power Sources* **2008**, *183*, 34−42.
(10) Jaouen, F.; Herranz, J.; Lefèvre, M.; Dodelet, J. P.; Kramm, U. I.; Herrmann, I.; Bongandoff, P.; Maruyama, J.; Nagaoka, T.; Garsuch, A.; et al. *ACS Appl. Mater. Interfaces* **2009**, *1*, 1623−1629.
(11) Lefèvre, M.; Proietti, E.; Jaouen, F.; Dodelet, J. P. *Science* **2009**, *324*, 71−74.
(12) Wu, G.; More, K. L.; Johnston, C. M.; Zelenay, P. *Science* **2011**, *332*, 443−447.
(13) Jaouen, F.; Proietti, E.; Lefèvre, M.; Chenitz, R.; Dodelet, J. P.; Wu, G.; Chung, H. T.; Johnston, C. M.; Zelenay, P. *Energy Environ. Sci.* **2011**, *4*, 114−130.
(14) Morozan, A.; Jousselme, B.; Palacin, S. *Energy Environ. Sci.* **2011**, *4*, 1238−1254.
(15) Bronzgou, A.; Song, S. Q.; Tsiakaras., P. *Appl. Catal., B* **2012**, *127*, 371−388.
(16) Niwa, H.; Horiba, K.; Harada, Y.; Oshima, M.; Ikeda, T.; Terakura, K.; Ozaki, J.; Miyata, S. *J. Power Sources* **2009**, *187*, 93−97.
(17) Gong, K.; Du, F.; Xia, Z.; Durstock, M.; Dai, L. *Science* **2009**, *323*, 760−764.
(18) Iwazaki, T.; Yang, H.; Obinata, R.; Sugimoto, W.; Takasu, Y. *J. Power Sources* **2010**, *195*, 5840−5847.
(19) Morozan1, A.; Jégou1, P.; Pinault, M.; Campidelli, S.; Jousselme, B.; Palacin, S. *ChemSusChem* **2012**, *5*, 647−651.
(20) Wohlgemuth, S. A.; White, R. J.; Willinger, M. G.; Titirici, M. M.; Antonietti, M. *Green Chem.* **2012**, *14*, 1515−1523.
(21) Choi, C. H.; Park, S. H.; Woo, S. I. *ACS Nano* **2012**, *6*, 7084−7091.
(22) Takasu, Y.; Suzuki, M.; Yang, H.; Ohashi, T.; Sugimoto, W. *Electrochem. Acta* **2010**, *55*, 8220−8229.
(23) Ishihara, A.; Lee, K.; Doi, S.; Mitsushima, S.; Kamiya, N.; Hara, M.; Domen, K.; Fukuda, K.; Ota, K. *Electrochem. Solid-State Lett.* **2005**, *8*, A201−A203.
(24) Ishihara, A.; Shibata, Y.; Mitsushima, S.; Ota, K. *J. Electrochem. Soc.* **2008**, *155*, B400−B406.
(25) Nam, K. D.; Ishihara, A.; Matsuzawa, K.; Mitsushima, S.; Ota, K.; Matsumoto, M.; Imai, H. *Electrochim. Acta* **2010**, *55*, 7290−7297.
(26) Ohgi, Y.; Ishihara, A.; Matsuzawa, K.; Mitsushima, S.; Ota, K. *J. Electrochem. Soc.* **2010**, *157*, B885−B891.
(27) Ohnishi, R.; Takahashi, Y.; Takagaki, A.; Kubota, J.; Domen, K. *Chem. Lett.* **2008**, *37*, 838−839.
(28) Ohnishi, R.; Katayama, M.; Takanabe, K.; Kubota, J.; Domen, K. *Electrochim. Acta* **2010**, *55*, 5393−5400.
(29) Yin, F.; Takanabe, K.; Kubota, J.; Domen, K. *J. Electrochem. Soc.* **2010**, *157*, B240−B244.
(30) Yin, F.; Takanabe, K.; Katayama, M.; Kubota, J.; Domen, K. *Electrochem. Commun.* **2010**, *12*, 1177−1179.
(31) Ou, Y.; Kumagai, H.; Yin., F.; Okada, S.; Hatasawa, H.; Morioka, H.; Takanabe, K.; Kubota, J.; Domen, K. *J. Electrochem. Soc.* **2011**, *158*, B1491−B1498.
(32) Seo, J.; Cha, D.; Takanabe, K.; Kubota, J.; Domen, K. *Chem. Commun.* **2012**, *48*, 9074−9076.
(33) Chen, J.; Takanabe, K.; Ohnishi, R.; Lu, D.; Okada, S.; Hatasawa, H.; Morioka, H.; Antonietti, M.; Kubota, J.; Domen, K. *Chem. Commun.* **2010**, *46*, 7492−7494.
(34) Isogai, S.; Ohnishi, R.; Katayama, M.; Kubota, J.; Kim, D. Y.; Noda, S.; Cha, D.; Takanabe, K.; Domen, K. *Chem.−Asian J.* **2012**, *7*, 286−289.
(35) Takagaki, A.; Takahashi, Y.; Yin, F.; Takanabe, K.; Kubota, J.; Domen, K. *J. Electrochem. Soc.* **2009**, *156*, B811−B815.
(36) Marković, N. M.; Schmidt, T. J.; Stamenković, V.; Ross, P. N. *Fuel Cells* **2001**, *1*, 105−116.
(37) Nørskov, J. K.; Rossmeisl, J.; Logadottir, A.; Lindqvist, L.; Kitchin, J. R.; Bligaard, T.; Jónsson, H. *J. Phys. Chem. B* **2004**, *108*, 17886−17892.
(38) Anderson, A. B.; Roques, J.; Mukerjee, S.; Murthi, V. S.; Markovic, N. M.; Stamenkovic, V. *J. Phys. Chem. B* **2005**, *109*, 1198−1203.
(39) Jacob, T. *Fuel Cells* **2006**, *6*, 159−181.
(40) Janik, M. J.; Taylor, C. D.; Neurock, M. *J. Electrochem. Soc.* **2009**, *156*, B126−B135.
(41) Tripkovíc, V.; Skúlason, E.; Siahrostami, S.; Nørskov, J. K.; Rossmeisl, J. *Electrochim. Acta* **2010**, *55*, 7975−7981.
(42) Redhead, P. A. *Vacuum* **1962**, *12*, 203−211.
(43) de-Jong, A. M.; Niemantsverdriet, J. W. *Surf. Sci.* **1990**, *233*, 355−365.
(44) Gland, J. L. *Surf. Sci.* **1980**, *93*, 487−514.
(45) Gland, J. L.; Sexton, B. A.; Fisher, G. B. *Surf. Sci.* **1980**, *95*, 587−602.
(46) Katada, N.; Igi, H.; Kim, J. H.; Niwa, M. *J. Phys. Chem. B* **1997**, *101*, 5969−5977.
(47) Kahlich, M. J.; Gasteiger, H. A.; Behm, R. J. *J. Catal.* **1997**, *171*, 93−105.
(48) Iwamoto, M.; Yahiro, H.; Tanda, K.; Mizuno, N.; Mine, Y.; Kagawa, S. *J. Phys. Chem.* **1991**, *95*, 3727−3730.
(49) Fischer, A.; Antonietti, M.; Thomas, A. *Adv. Mater.* **2007**, *19*, 264−267.
(50) Yuliati, L.; Yang, J. H.; Wang, X.; Maeda, K.; Takata, T.; Antonietti, M.; Domen, K. *J. Mater. Chem.* **2010**, *20*, 4295−4298.
(51) Fukasawa, Y.; Takanabe, K.; Shimojima, A.; Antonietti, M.; Domen, K.; Okubo, T. *Chem.−Asian J.* **2011**, *6*, 103−109.
(52) Wang, Y.; Ohnishi, R.; Yoo, E.; He, P.; Kubota, J.; Domen, K.; Zhou., H. *J. Mater. Chem.* **2012**, *22*, 15549−15555.